Geomech. Geophys. Geo-energ. Geo-resour. (2024) 10:84
https://doi.org/10.1007/s40948-024-00806-5

RESEARCH

Experimental study on the influence of external fluids on the pore structure of carbonaceous shale

Ying Yang · Jianguang Wei · Yinhua Liu · Quanshu Zeng · Jingde Lin · Jiangtao Li

Received: 28 September 2023 / Accepted: 25 April 2024

Abstract Shale reservoirs have complex mineral compositions and are rich in micro-scale pores. It is of great scientific and engineering significance to explore the mechanism of external fluids on the pore throat structure of shale. In this paper, pure carbonaceous shale is taken as the research object, and the mechanism of the influence of slip water and reflux fluid on the pore throat structure is analyzed by using nuclear magnetic resonance (NMR) technology. Then, the sensitivity of different types of shale to external fluids is comparatively analyzed and summarized. The results show that (1) the oil slick has a certain effect on the total porosity of different types of shale. The rate of change is shown as carbonaceous shale (−7.1%) > pure shale (−1.6%). (b) For slick-water, the average reduction of macro- and micro/nanopores in carbonaceous shale is 90.0% and 5.0%, respectively, while the average reduction of macro- and mesopores in pure shale is 17.7% and 6.8%, respectively. (c) Total porosity of different shale types is insensitive to refluxing fluids. The average increase in macro-, meso-, and small pores of carbonaceous shale is 31.8%, 23.6%, and 20.2%, respectively; the average increase in macro- and small pores of pure shale is 17.1%.

Keywords Carbonaceous shale · Pore throat structure · Variable viscosity slick water · Backflow fluid · Nuclear magnetic resonance

Y. Yang · J. Wei (✉) · J. Li
National Key Laboratory of Continental Shale Oil, Northeast Petroleum University, Northeast Petroleum University, Daqing 163318, Heilongjiang, China
e-mail: weijianguang@163.com

Y. Yang · J. Wei · J. Li
Unconventional Oil and Gas Research Institute, Northeast Petroleum University, Daqing 163318, China

Y. Liu · J. Lin
Engineering Technology Research Institute, PetroChina Coalbed Methane Company Limited, Xi'an 710082, China

Y. Liu · J. Lin
China United Coalbed Methane National Engineering Research Center Co. Ltd., Beijing 100095, China

Q. Zeng
Department of Petroleum Engineering, China University of Petroleum, Beijing, China

1 Introduction

With the increasing demand for oil and gas resources and the depletion of conventional oil and gas resources (Liu et al. 2020a, b, 2023a), unconventional oil and gas resources have become more important (Chen et al. 2023; Cui et al. 2023; Liu et al. 2021). Shale oil and gas are a crucial part of unconventional oil and gas resources (Liu et al. 2020c, 2019; Gao et al. 2023), driving global energy structure reform (Sun et al. 2018a, 2017; Meng et al. 2023a; Jiang et al. 2022). Shale oil and gas resources refer to the oil and natural gas resources stored in shale formations

Published online: 03 May 2024

(Tao et al. 2023; Li et al. 2023). Shale is not only the source rock of oil and gas resources (Yu et al. 2023; Meng et al. 2023b; Lu et al. 2020; Ma et al. 2019), but also the reservoir rock of oil and gas resources (Liu et al. 2023b; Nie 2023; Yuan et al. 2023; Sun et al. 2018b). The mineral composition of shale reservoirs is complex (Shao et al. 2023; Shi et al. 2022; Sun et al. 2018d), and the impact mechanisms of various minerals on different fluids vary greatly (Wei et al. 2023a; Wei and Sheng 2022; Xie et al. 2022). In addition, the pore throat structure of shale is dense and the connectivity is complex (Yang et al. 2022a, 2022b; Liu et al. 2023c; Sun et al. 2019a). Exploring the mechanism of external fluid action in the pore throat structure has important scientific and engineering significance (Yang et al. 2023a; Liu et al. 2023d; Sun et al. 2019b).

Wei et al. (2023b) studied the spontaneous infiltration mechanism of shale and found that the pore throat structure has a significant impact on the infiltration of external fluids. Xie et al. (2023) studied the establishment method of three-dimensional digital shale core and analyzed the influence of microscale fractures on fluid infiltration. Lai et al. (2023) analyzed the stability of complex drilling fluids, providing basic parameters for establishing a fracturing fluid infiltration model. Wang et al. (2022a) analyzed the damage mechanism of fracturing fluid on pore throat structure and established a coupling model between pore throat structure and fracturing fluid. Yang et al. (2023b) established a classification system for fracturing fluids based on their filtration characteristics and explored the mechanical changes of continental shale along the longitudinal profile. Yang et al. (2023a) established a fluid structure coupling model for shale microscale and nanoscale pore throat structure and analyzed the influence of different nanofiber structures on the sealing effect. Zhou et al. (2022) studied the effect of hydration on the infiltration and absorption of external fluids from shale, and analyzed the spontaneous infiltration and absorption mechanism during the well closure process. Guo et al. (2018) studied the effect of polymer adsorption on pore throat properties in slick water, and analyzed the coupling relationship between adsorption concentration, pH, and polymer concentration. Zhou et al. (2024) studied the influence of external fluids on the pore throat structure of tight reservoirs and analyzed the evolution mechanism of permeability. Yang et al. (2022c) studied the influence of mineral types and pore throat structure on the flow pattern, and analyzed three flow patterns in porous media. Wang et al. (2022b) established a gas water infiltration exchange model based on the gas water interaction mode and conducted application analysis in shale reservoirs. Ding et al. (2023) studied the effect of clay minerals on infiltration and found that the fracturing fluid first entered microscale pores. Chen et al. (2020) studied the damage mechanism of water phase capture on shale reservoirs and analyzed the impact of salinity. Namaee-Ghasemi et al. (2023) studied the interaction mode between low salinity water injection and pore throat structure, and explored the evolution characteristics of contact angle based on the concept of separation pressure.

In summary, many scholars have explored the sensitivity of shale reservoirs to external fluids (Xiao et al. 2023; Assal et al. 2023; Guo et al. 2023), but there is relatively little comparative research on slick water and backflow fluid, and systematic experimental research on the sensitivity of carbonaceous shale has not yet been conducted (Elbahrawy et al. 2023; Hou et al. 2023; Men et al. 2023). Therefore, in this paper, shale core samples are selected from the Daning-Jixian block in the eastern edge of the Ordos Basin, China, and sensitivity evaluation experiments are conducted on external fluids (slick water and backflow fluid) with different types of shale microscale pore structures. Firstly, taking pure shale as the research object, the influence mechanism of slick water and backflow fluid on the pore throat structure of pure shale is explored. On this basis, taking carbonaceous shale as the research object, the mechanism of the influence of slick water and backflow fluid on the pore throat structure of carbonaceous shale is analyzed. Finally, a comparative analysis and summary are conducted on the sensitivity of different types of shale to external fluids. The research results of this article have guiding significance for the formulation of fracturing fluid and the design of fracturing process. At the same time, it provides basic analysis parameters for revealing the gas/water dynamic characteristics of infiltration/production during fracturing process of shale reservoirs.

2 Evaluation method for sensitivity of shale pore structure to external fluids.

In this paper, the high-frequency and low-field nuclear magnetic resonance instrument is used to conduct two-dimensional nuclear magnetic T_2 spectrum testing on saturated formation water cores and saturated external fluids (such as slick water and backflow fluid) cores. According to the T_2 spectrum, divide the bound water in organic matter and clay and extract the T_2 spectrum of fluid signals in the pore space of the rock core. For saturated fluid cores, the T_2 value is linearly related to the pore radius r, i.e. $T_2 = k \cdot r$. By comparing the T_2 spectrum of fluid signals in the pore space of the rock core with the high-pressure mercury injection pore throat distribution test results of parallel samples, the conversion of T_2 values to pore radius can be achieved, and the pore structure of the rock core can be determined based on the T_2 spectrum of fluid signals in the pore space of the rock core, and therefore, quantitative identification of porosity and movable fluids corresponding to different sizes of pores (<0.0l μm micropores; 0.01–0.1 μm small pores; 0.1–1.0 μm medium pores; >1.0 μm large pores) before and after immersion in external fluids in shale cores has been achieved. At the same time, sensitivity evaluation indicators for shale pores of different sizes are established: total porosity change rate, microporous porosity change rate, small pore porosity change rate, mesoporous porosity change rate, and macropore porosity change rate. Finally, a quantitative evaluation of the sensitivity of pores of different sizes in carbonaceous shale to external fluids is achieved.

3 Sensitivity experiment of external fluids in pore structure.

Based on two-dimensional nuclear magnetic resonance testing technology, identification of movable fluids and microscopic pore structure characteristics in shale gas reservoirs can be achieved. By comparing and analyzing the characteristic changes in the movable fluid and microscale pore structure of shale gas reservoir cores before and after immersion in external fluids (such as slick water and backflow fluid), the sensitivity of the reservoir to external fluids can be evaluated. In this section, the experimental equipment, experimental conditions, and experimental steps are introduced.

3.1 Experimental materials, conditions, and equipment.

For the sensitivity evaluation experiment of shale pore structure to foreign fluids, different concentrations of neutral sliding water and backflow fluid are selected as external fluids. The density of neutral slick water (0.4% lotion drag reducer + 0.1% drainage aid + 0.06% APS) is 1.005 g/ml; the density of the backflow liquid is 1.070 g/ml; the temperature is 71.8 °C; The experimental pressure is 18 MPa; the density of formation water is 1.101 g/ml. The selected core foundation parameters and experimental plan are detailed in Table 1. It should be noted that in order to reveal the influence of foreign fluids on carbonaceous shale, pure shale is also studied to enhance contrast. As shown in Table 1. The first to fourth groups are sensitivity evaluation experiments for external fluids in pure shale, while the fifth to eighth groups are sensitivity evaluation experiments for external fluids in carbonaceous shale.

The experimental equipment and instruments mainly include: high-precision desktop two-dimensional nuclear magnetic resonance instrument, high-temperature and high-pressure displacement device, high-pressure mercury intrusion meter, X-ray diffractometer, one thousandth high-precision balance, hand pump, pressure gauge, and core gripper.

3.2 Experimental methods and steps.

Based on the established method for evaluating the sensitivity of shale gas reservoir pore structure to external fluids, experimental steps for evaluating the sensitivity of shale gas reservoir pore structure have been developed:

(a) Prepare rock cores columns with a diameter of 2.5 cm and a length of 5 cm using a wire cutting instrument. The remaining samples are subjected to high-pressure mercury intrusion and XRD testing. Prepare formation water and external fluids (slick water, backflow fluid) for the experiment.
(b) Shale cores are dried to constant weight at 60 °C (with no change in mass after 4 h) and subjected to nuclear magnetic resonance testing.

Table 1 Basic parameters and experimental plan of rock cores

No	Shall type	Core No	Length/cm	Diameter /cm	Mass/g	Gas measured permeability/ mD	Test fluid
1	Pure shale	4–13–3–1	4.394	2.490	52.6644	0.0440	Slick water with variable viscosity (0.4%)
2	Pure shale	4–13–6–2	4.082	2.488	48.7768	0.0109	Backflow liquid
3	Pure shale	24–5–1–1	4.020	2.520	51.5634	0.1942	Slick water with variable viscosity (0.4%)
4	Pure shale	40–3–2	4.180	2.526	53.8308	0.3543	Backflow liquid
5	Carbonaceous shale	3–4–2–2	5.380	2.454	41.5771	5.5540	Slick water with variable viscosity (0.4%)
6	Carbonaceous shale	3–4–2–1	5.100	2.492	47.3796	6.1837	Backflow liquid
7	Carbonaceous shale	44–3–1	4.090	2.530	35.5366	0.1343	Slick water with variable viscosity (0.4%)
8	Carbonaceous shale	44–4–2	4.120	2.528	33.5183	0.0188	Backflow liquid

(c) Place the rock cores into a rock core gripper (with a confining pressure of 2 MPa) and vacuum it for 48 h. Under the conditions of reservoir temperature (71.8 °C) and pressure (18 MPa), saturate cores with formation water. Remove the rock cores, weigh it, and perform nuclear magnetic resonance testing.

(d) Dry the rock cores at 60 °C to a constant weight.

(e) Insert the rock cores into the gripper and apply a confining pressure of 2 MPa. After vacuuming for 48 h, saturate cores with external fluid. Conduct external fluid immersion experiments under reservoir temperature (71.8 °C) and pressure (18 MPa) conditions. After 48 h of experiment, the rock cores are taken out for weighing and nuclear magnetic resonance testing.

(f) Dry the rock core at 60 °C to constant weight and conduct XRD testing.

(g) Repeat steps (a)–(f) to conduct experiments on the sensitivity of different types of shale cores to different external fluids.

(h) Clarify the changes in mineral composition of the cores before and after the experiment. Quantify the porosity and movable fluids corresponding to different pore sizes (< 0.0l μm micropores; 0.01–0.1 μm small pores; 0.1–1.0 μm medium pores; > 1.0 μm large pores) in shale cores after saturation with formation water and external fluids (such as slick water and backflow fluid). Based on the established sensitivity evaluation indicators for shale pores of different sizes, quantitatively evaluate the sensitivity of shale pores of different sizes to external fluids.

4 Results and discussion

4.1 Sensitivity of pure shale pore structure to variable viscosity slick water.

The influence of variable viscosity slick water on the pore structure of pure shale is studied using core 24–5–1–1 and core 4–13–3–1. Figure 1 shows the T_2 spectrum of pure shale under dry samples, saturated formation water, and variable viscosity slick water conditions. As mentioned earlier, by comparing the T_2 spectrum of fluid signals in the pore spaces of core 24–5–1 and core 4–13–3–1 with the high-pressure mercury injection pore throat distribution test results of their parallel samples, the conversion of T_2 value to pore radius can be achieved. Furthermore, the pore structure of the shale core can be determined based on the T_2 spectrum of fluid signals in the pore space, achieving quantitative identification of porosity and movable fluids corresponding to different sizes (< 0.0l μm micropores; 0.01–0.1 μm small pores; 0.1–1.0 μm medium pores; > 1.0 μm large pores) of pores before and after immersion in external fluids. The relationship between the obtained pore distribution and relaxation time is shown in Fig. 2.

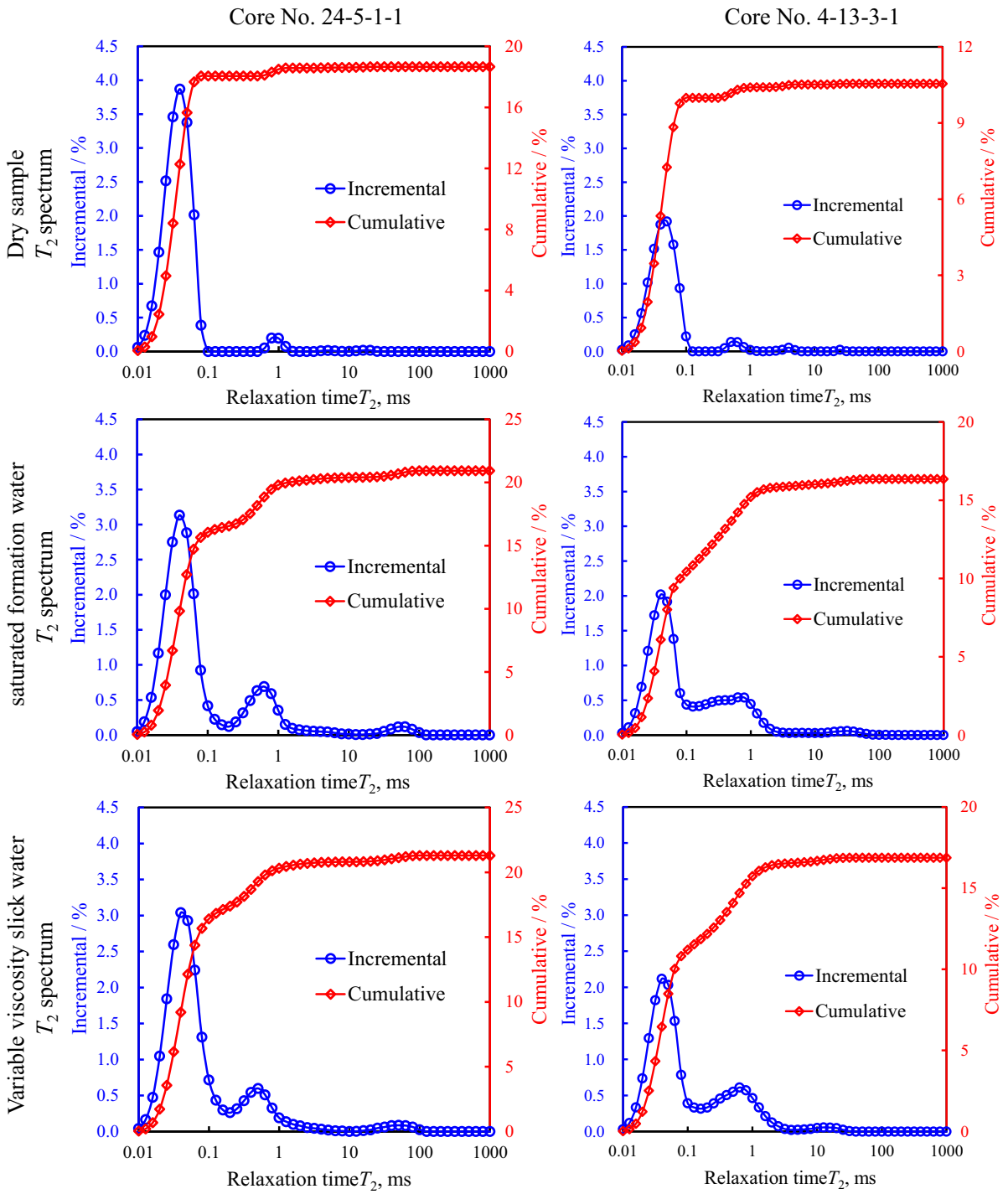

Fig. 1 T_2 spectrum of pure shale samples (core 24–5–1–1 and core 4–13–3–1) under dry, saturated formation water, and variable viscosity slick water conditions

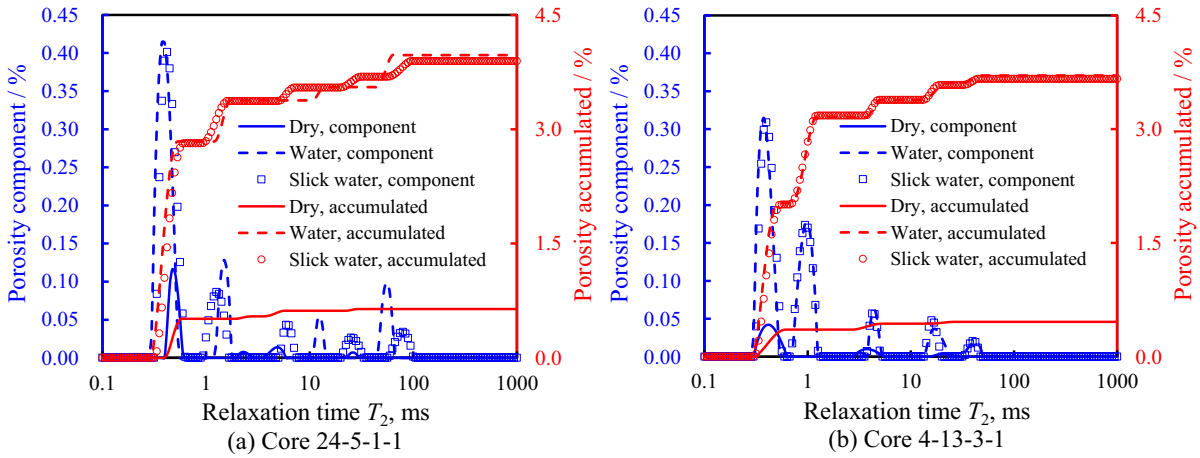

Fig. 2 Pore distribution characteristics of pure shale samples (core 24–5–1–1 and core 4–13–3–1) in their initial state and after soaking in variable viscosity slick water

Figure 2 shows the pore distribution characteristics of pure shale samples (core 24–5–1–1 and core 4–13–3–1) in their initial state and after soaking in slick water. It can be found from Fig. 2 that (a) the total porosity of pure shale decreases after the action of slick water. The total porosity of core 24–5–1–1 and core 4–13–3–1 after saturated formation water is 3.97% and 3.71%, respectively. The total porosity after saturation with variable viscosity slick water is 3.89% and 3.66%, respectively, reducing by 0.08% and 0.05%. (b) The decrease in total porosity refers to a decrease in the porosity of the fluid, which are 2.03% and 1.24%, respectively. (c) After the interaction between pure shale and variable viscosity slick water, the number of small pores increases, while the porosity of microscale and nanoscale pores, mesopores, and macropores slightly decreases.

Table 2 presents the quantitative characterization results of pore distribution in core 24–5–1–1 and core 4–13–3–1 after soaking in variable viscosity slick water. It can be seen from Table 2 that (a) the interaction between pure shale and slick water leads to an increase in nanoporous porosity, while the porosity of small, medium, and large pores decreases. (b) After

Table 2 The distribution of pore throats of different sizes in core 24–5–1–1 and core 4–13–3–1 before and after soaking in variable viscosity slick water

Core No	Soaking fluid	Pore parameters	Distribution of pore throats of different sizes within the rock core				
			< 0.01 μm	0.01–0.1 μm	0.1–1 μm	> 1 μm	Total
24–5–1–1	Formation water	Porosity (pore volume/apparent core volume)%	2.77	0.61	0.12	0.47	3.97
		Porosity ratio (pore volume/total pore volume)%	69.80	15.25	3.05	11.90	100
	Slick water	Porosity (pore volume/apparent core volume)%	2.75	0.63	0.12	0.39	3.89
		Porosity ratio (pore volume/total pore volume)%	70.78	16.09	3.14	9.99	100
4–13–3–1	Formation water	Porosity (pore volume/apparent core volume)%	1.90	1.46	0.23	0.11	3.71
		Porosity ratio (pore volume/total pore volume)%	51.31	39.45	6.28	2.96	100
	Slick water	Porosity (pore volume/apparent core volume)%	1.88	1.49	0.20	0.09	3.66
		Porosity ratio (pore volume/total pore volume)%	51.46	40.63	5.44	2.47	100

Table 3 Evaluation results of the sensitivity of pore structures in core 24–5–1–1 and core 4–13–3–1 to variable viscosity slick water

Core No	Soaking fluid	Evaluating indicator	I	Imic (< 0.01 μm)	Imc (0.01 ~ 0.1 μm)	Ime (0.1 ~ 1 μm)	Ima (> 1 μm)
24–5–1–1	Slick water	Indicator value	− 2.03	− 0.65	3.40	0.83	− 17.79
		Impact level	None	None	None	None	Weak (damage)
4–13–3–1	Slick water	Indicator value	− 1.24	− 0.95	1.73	− 14.48	− 17.66
		Impact level	None	None	None	Weak (damage)	Weak (damage)

saturation with formation water, the mesoporous porosity of core 24–5–1–1 and core 4–13–3–1 are 0.12% and 0.23%, respectively; After saturation with variable viscosity slick water, the mesoporous porosity are 0.12% and 0.20% respectively, and the change values of mesoporous porosity are 0% and − 0.03%, with a change rate of − 14.48% to 0.83%. (c) After saturation with formation water, the macroporous porosity of core 24–5–1–1 and core 4–13–3–1 are 0.47% and 0.11%, respectively; After saturation with variable viscosity slick water, the macropore porosity are 0.39% and 0.09% respectively, and the variation values of macropore porosity are − 0.08% and − 0.02%, with a decrease of 17.66 to 17.79%. (d) Core 24–5–1–1 and core 4–13–3–1 showed a decrease of 0.02% and 0.02% in micropores and small pores, respectively, after the action of slick water. The decrease in micropores is 0.65% to 0.95%, while the increase in small pores is 1.73% to 3.40%.

Table 3 summarizes the evaluation results of the sensitivity of the pore structure of core 24–5–1–1 and core 4–13–3–1 to slick water. It can be found from Table 3 that slick water is not sensitive to total porosity, and is not sensitive to microsclae and nanoscale pores and small pores, causing weak damage to mesopores and large pores. In summary, the research results indicate that slick water is not sensitive to the total porosity of pure shale, and is not sensitive to microscale and nanoscale pores and small pores. It has a slight impact on porosity, causing weak damage to mesopores and large pores, leading to a significant decrease in porosity.

4.2 Sensitivity of pure shale pore structure to backflow fluid.

The influence of backflow fluid on the pore structure of pure shale is studied using core 40–3–2 and core 4–13–6–2. Figure 3 shows the T_2 spectrum of pure shale under dry samples, saturated formation water, and backflow fluid conditions. As mentioned earlier, by comparing the T_2 spectrum of fluid signals in the pore spaces of core 40–3–2 and core 4–13–6–2 with the high-pressure mercury injection pore throat distribution test results of their parallel samples, the conversion of T_2 value to pore radius can be achieved. Furthermore, the pore structure of the shale core can be determined based on the T_2 spectrum of fluid signals in the pore space, achieving quantitative identification of porosity and movable fluids corresponding to different sizes (< 0.0l μm micropores; 0.01–0.1 μm small pores; 0.1–1.0 μm medium pores; > 1.0 μm large pores) of pores before and after immersion in external fluids. The relationship between the obtained pore distribution and relaxation time is shown in Fig. 4.

Figure 4 shows pore distribution characteristics of pure shale samples (core 40–3–2 and core 4–13–6–2) in their initial state and after soaking in backflow fluid. As shown in Fig. 4, (a) the total porosity of pure shale increases after saturated with backflow fluid. The total porosity of core 40–3–2 and core 4–13–6–2 after saturated with formation water are 4.16% and 3.60%, respectively. (b) The total porosity after saturated with backflow fluid are 4.22% and 3.66%, respectively, with an increase of 0.06% and 0.06%. (c) The increase in total porosity refers to an increase in the porosity of the fluid, which are 1.85% and 1.43%, respectively.

Table 4 presents the quantitative characterization results of pore distribution in core 40–3–2 and core 40–13–6–2 after soaking in backflow fluid. According to Table 4, it can be seen that (a) after the interaction of pure shale and backflow fluid, the macroscale pore porosity increases, while the microscale and nanoscale pore, small pore, and mesoscale pore porosity slightly decrease. (b) The macroscale pore porosity of core 40–3–2 and

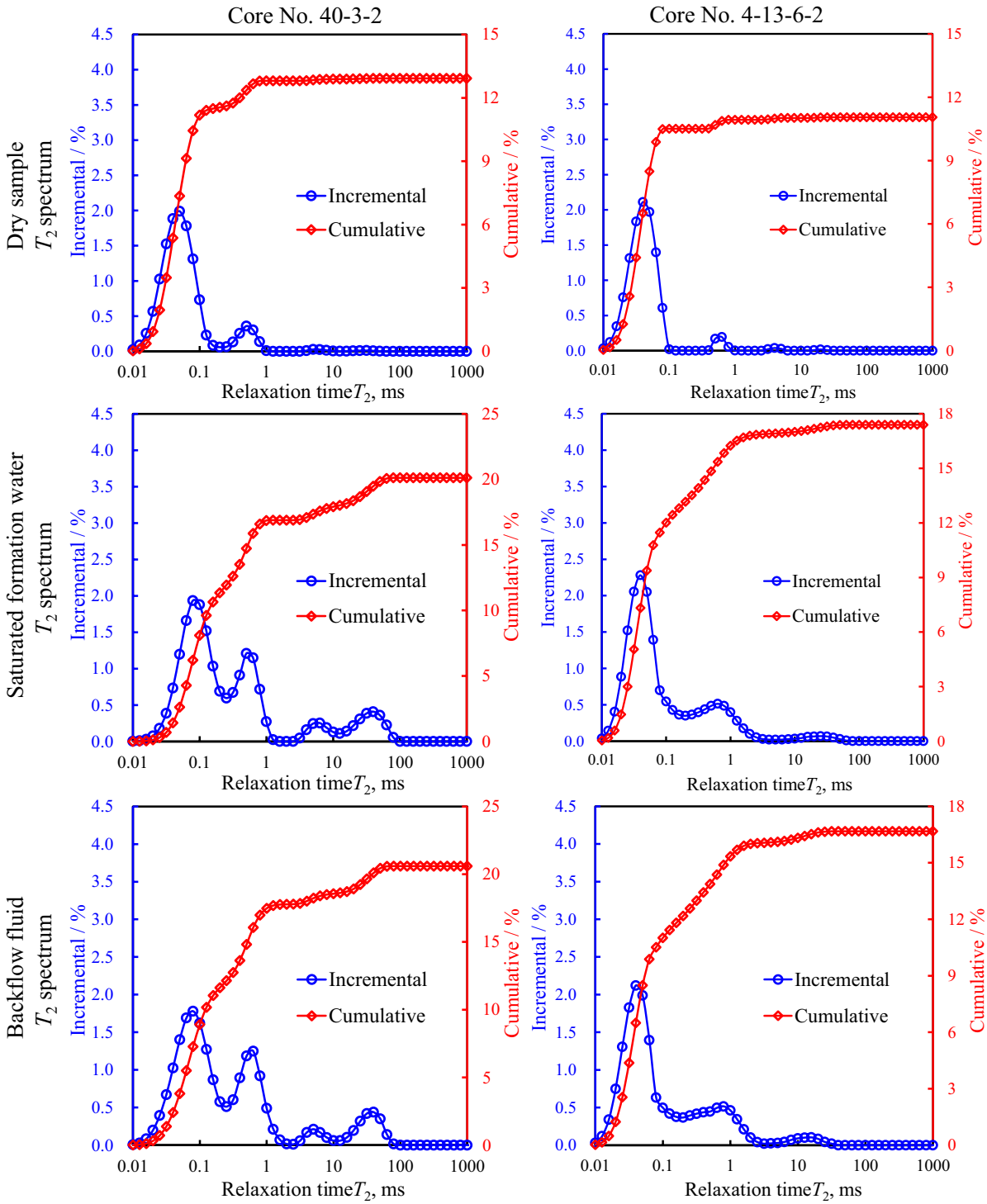

Fig. 3 T_2 spectrum of pure shale samples (core 40–3–2 and core 4–13–6–2) under dry, saturated formation water, and backflow fluid conditions

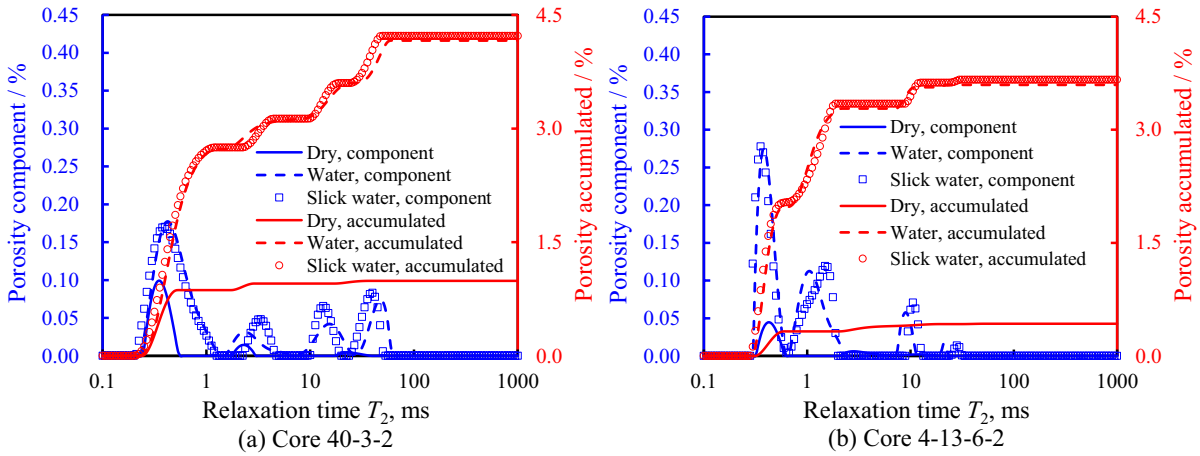

Fig. 4 Pore distribution characteristics of pure shale samples (core 40–3–2 and core 4–13–6–2) in their initial state and after soaking in backflow fluid

Table 4 The distribution of pore throats of different sizes in core 24–5–1–1 and core 4–13–3–1 before and after soaking in backflow fluid

Core No	Soaking fluid	Pore parameters	Distribution of pore throats of different sizes within the rock core				
			< 0.01 μm	0.01–0.1 μm	0.1–1 μm	> 1 μm	Total
40–3–2	Formation water	Porosity (pore volume/apparent core volume)%	2.44	0.40	0.61	0.71	4.16
		Porosity ratio (pore volume/total pore volume)%	58.60	9.69	14.62	17.09	100
	Backflow fluid	Porosity (pore volume/apparent core volume)%	2.46	0.39	0.59	0.79	4.22
		Porosity ratio (pore volume/total pore volume)%	58.17	9.13	13.95	18.76	100
4–13–6–2	Formation water	Porosity (pore volume/apparent core volume)%	1.87	1.44	0.25	0.03	3.60
		Porosity ratio (pore volume/total pore volume)%	52.12	40.17	6.94	0.78	100
	Backflow fluid	Porosity (pore volume/apparent core volume)%	1.94	1.44	0.24	0.03	3.66
		Porosity ratio (pore volume/total pore volume)%	53.02	39.35	6.69	0.94	100

core 4–13–6–2 saturated with formation water are 0.71% and 0.03%, respectively. (c) The macroscale pore porosity after saturated with backflow fluid are 0.79% and 0.03%, respectively. The variation values of macroscale pore porosity are 0.08% and 0.01%, with an increase of 11.29–22.99%. (d) The microscale pore porosity of core 24–5–1–1 and core 4–13–3–1 increased by 0.02–0.07% after saturation with slick water; The porosity of small pores and mesoscale pores decreased by 0.02–0% and 0–0.02%, respectively. The decrease in microscale pore is 0.68–3.61%, the decrease in small pore is 0.21–4.42%, and the decrease in mesoscale pore is 1.80–3.25%.

Table 5 summarizes the evaluation results of the sensitivity of the pore structure of cores 40–3–2 and 4–13–6–2 to backflow fluids. According to Table 5, it can be seen that the backflow fluid is not sensitive to the total porosity, is not sensitive to microscale, nanoscale, small, and medium pores, and has weak improvement on large pores. In summary, the results of this study indicate that the total porosity of pure

Table 5 Evaluation results of the sensitivity of pore structures in core 40–3–2 and core 4–13–6–2 to backflow fluid

Core No	Soaking fluid	Evaluating indicator	I	Imic (< 0.01 μm)	Imc (0.01–0.1 μm)	Ime (0.1–1 μm)	Ima (> 1 μm)
40–3–2	Backflow fluid	Indicator value	1.43	0.68	− 4.42	− 3.25	11.29
		Impact level	None	None	None	None	Weak (damage)
4–13–6–2	Backflow fluid	Indicator value	1.85	3.61	− 0.21	− 1.80	22.99
		Impact level	None	None	None	None	Weak (damage)

shale is not sensitive to backflow fluid, while microscale and nanoscale pores and small and medium pores are not sensitive to backflow fluids, with slight changes in porosity; backflow fluid has a weak improvement effect on macroscale pores, leading to a significant increase in porosity.

4.3 Sensitivity of carbonaceous shale pore structure to variable viscosity slick water.

The influence of variable viscosity slick water on the pore structure of carbonaceous shale is studied using core 3–4–2–2 and core 44–3–1. Figure 5 shows the T_2 spectrum of carbonaceous shale under dry samples, saturated formation water, and variable viscosity slick water conditions. As mentioned earlier, by comparing the T_2 spectrum of fluid signals in the pore spaces of core 3–4–2–2 and core 44–3–1 with the high-pressure mercury injection pore throat distribution test results of their parallel samples, the conversion of T_2 value to pore radius can be achieved. Furthermore, the pore structure of the shale core can be determined based on the T_2 spectrum of fluid signals in the pore space, achieving quantitative identification of porosity and movable fluids corresponding to different sizes (< 0.0l μm micropores; 0.01–0.1 μm small pores; 0.1–1.0 μm medium pores; > 1.0 μm large pores) of pores before and after immersion in external fluids. The relationship between the obtained pore distribution and relaxation time is shown in Fig. 6.

From Fig. 6, it can be seen that the total porosity of carbonaceous shale decreases after saturation with slick water. The total porosity of core 3–4 2–2 and core 44–3–1 after saturation with formation water are 6.85% and 4.14%, respectively; the total porosity after saturation with slick water are 6.28% and 3.90%, respectively, reducing by 0.57% and 0.24%. The decrease in total porosity refers to a decrease in the porosity of the fluid, which are 8.46% and 5.71%, respectively. After the interaction of carbonaceous shale with slick water, the porosity of microscale and nanoscale pore and macroscale pore decreases, while the porosity of small pore and mesoscale pore increases.

Table 6 presents the quantitative characterization results of pore distribution in core 3–4 2–2 and core 44–3–1 after soaking in slick water. According to Table 6, it can be seen that the interaction between carbonaceous shale and slick water leads to a decrease in microscale and nanoscale pore porosity, while the porosity of small, medium, and large pores increases. After saturation with formation water, the macroscale pore porosities of core 3–4 and core 44–3–1 are 0.63% and 0.18%, respectively; after saturation with slick water, the macroscale pore porosity are 0.10% and 0.01% respectively, and the variation values of macroscale pore porosity are − 0.53% and − 0.17%, with a decrease of 84.75–95.16%. Core 3–4 2–2 and core 44–3–1 showed a decrease of 0.20–0.23% in microscale pore porosity after saturation with slick water, while the microscale and mesoscale pores increased by 0.10% − 0.16% and 0.03%, respectively. The microscale pore decreased by 4.43–5.59%, the microscale pore increased by 7.81–12.53%, and the mesoscale pore increased by 3.95–5.52%.

Table 7 summarizes the evaluation results of the sensitivity of the pore structure of core 3–4–2–2 and core 44–3–1. According to Table 7, slick water is not sensitive to total porosity, and is not sensitive to microscale and nanoscale pores and small pores, causing weak damage in mesoscale pores and large pores. In summary, the results of this study indicate that slick water is not sensitive to the total porosity of carbonaceous shale, and is not sensitive to microscale and nanoscale pores and small pores, with

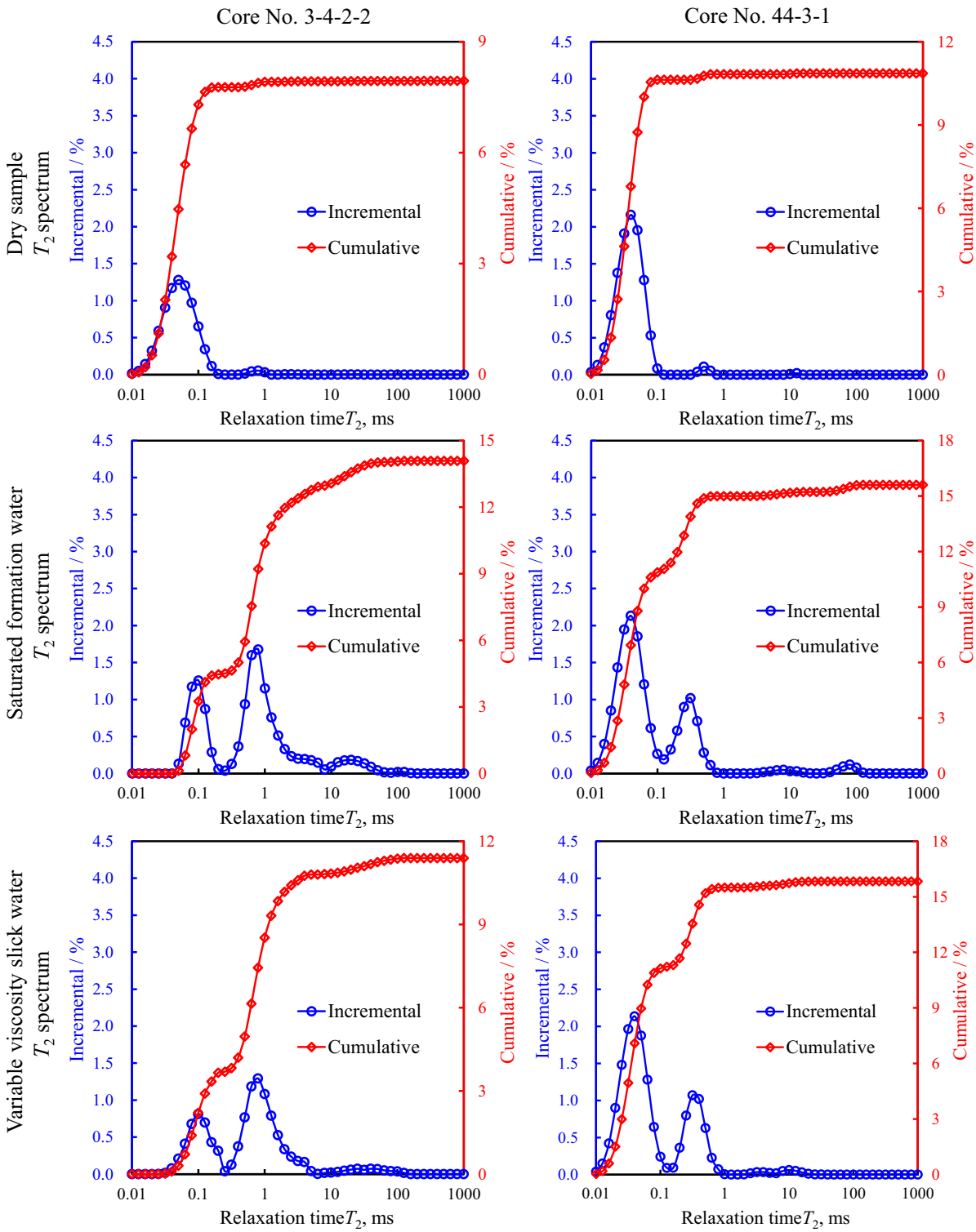

Fig. 5 T_2 spectrum of carbonaceous shale samples (core 3–4–2–2 and core 44–3–1) under dry, saturated formation water, and variable viscosity slick water conditions

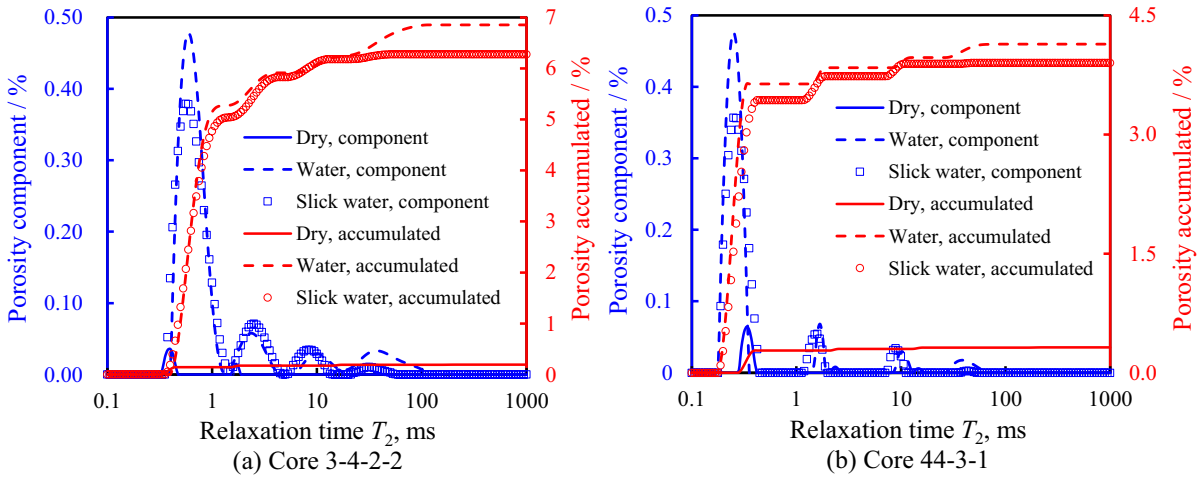

Fig. 6 Pore distribution characteristics of carbonaceous shale samples (core 3–4–2–2 and core 44–3–1) in their initial state and after soaking in variable viscosity slick water

Table 6 The distribution of pore throats of different sizes in core 3–4 2–2 and core 44–3–1 before and after soaking in variable viscosity slick water

Core No	Soaking fluid	Pore parameters	Distribution of pore throats of different sizes within the rock core				
			< 0.01 μm	0.01–0.1 μm	0.1–1 μm	> 1 μm	Total
3–4–2–2	Formation water	Porosity (pore volume/apparent core volume)%	5.28	0.63	0.32	0.63	6.85
		Porosity ratio (pore volume/total pore volume)%	77.02	9.17	4.62	9.20	100
	Slick water	Porosity (pore volume/apparent core volume)%	5.05	0.79	0.35	0.10	6.28
		Porosity ratio (pore volume/total pore volume)%	80.41	12.53	5.52	1.53	100
44–3–1	Formation water	Porosity (pore volume/apparent core volume)%	3.64	0.20	0.12	0.18	4.14
		Porosity ratio (pore volume/total pore volume)%	87.90	4.83	2.92	4.35	100
	Slick water	Porosity (pore volume/apparent core volume)%	3.43	0.30	0.15	0.01	3.90
		Porosity ratio (pore volume/total pore volume)%	88.02	7.81	3.95	0.22	100

Table 7 Evaluation results of the sensitivity of pore structures in core 3–4 2–2 and core 44–3–1 to variable viscosity slick water

Core No	Soaking fluid	Evaluating indicator	I	Imic (< 0.01 μm)	Imc (0.01 ~ 0.1 μm)	Ime (0.1 ~ 1 μm)	Ima (> 1 μm)
3–4–2–2	Slick water	Indicator value	− 8.46	− 4.43	25.17	9.34	− 84.75
		Impact level	Weak (damage)	None	Weak (improved)	Weak (improved)	Weak (damage)
4–13–3–1	Slick water	Indicator value	− 5.71	− 5.59	52.30	27.54	− 95.16
		Impact level	Weak (damage)	Weak (damage)	Moderately strong (improved)	Weak (improved)	Weak (damage)

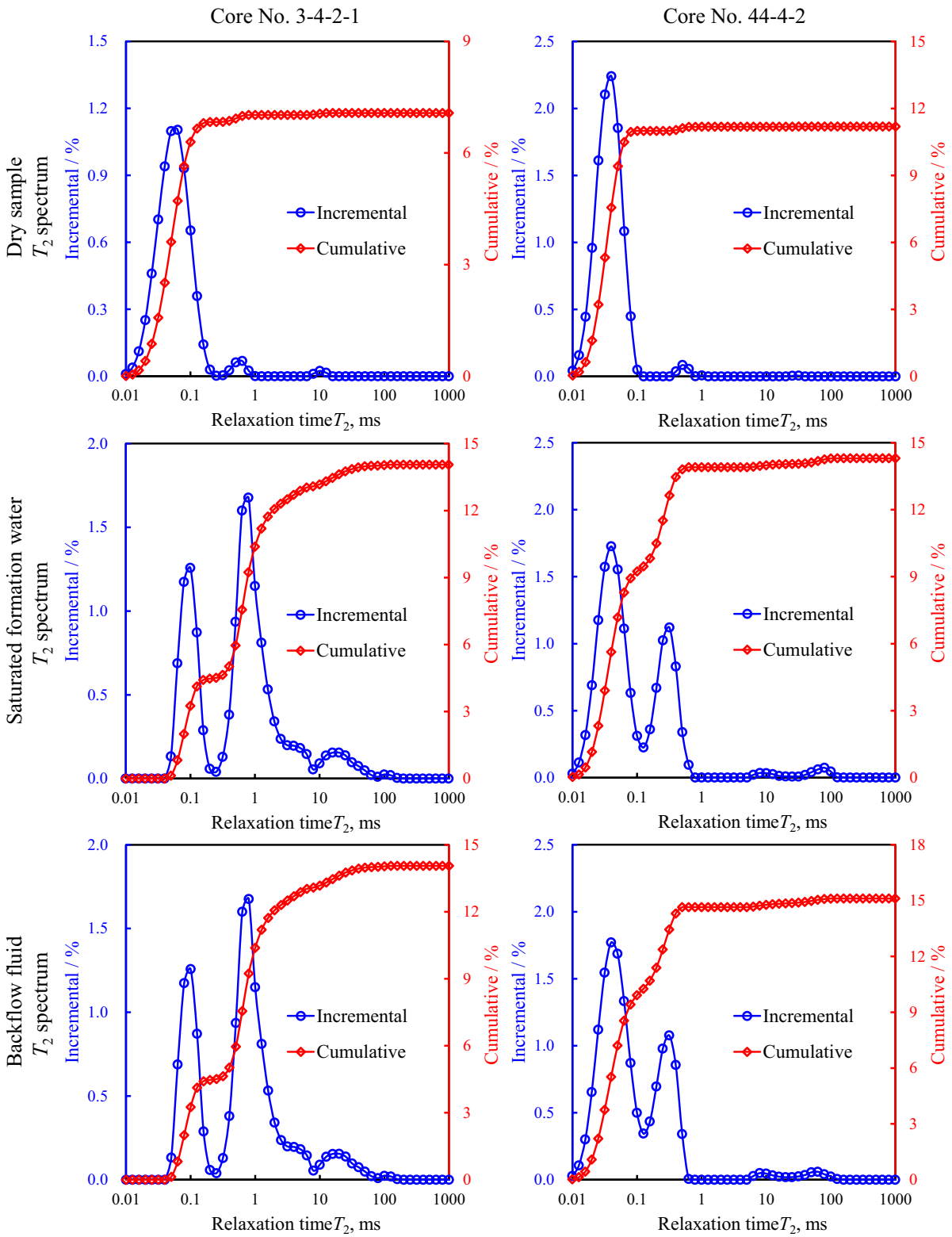

Fig. 7 T_2 spectrum of carbonaceous shale samples (core 3–4–2–1 and core 44–4–2) under dry, saturated formation water, and backflow fluid conditions

slight changes in porosity; slick water causes weak damage to mesoscale and macroscale pores, with a significant decrease in porosity.

4.4 Sensitivity of carbonaceous shale pore structure to backflow fluid.

The influence of backflow fluid on the pore structure of carbonaceous shale is studied using core 3–4–2–1 and core 44–4–2. Figure 7 shows the T_2 spectrum of carbonaceous shale under dry samples, saturated formation water, and backflow fluid conditions. As mentioned earlier, by comparing the T_2 spectrum of fluid signals in the pore spaces of core 3–4–2–1 and core 44–4–2 with the high-pressure mercury injection pore throat distribution test results of their parallel samples, the conversion of T_2 value to pore radius can be achieved. Furthermore, the pore structure of the shale core can be determined based on the T_2 spectrum of fluid signals in the pore space, achieving quantitative identification of porosity and movable fluids corresponding to different sizes (<0.0l μm micropores; 0.01–0.1 μm small pores; 0.1–1.0 μm medium pores; >1.0 μm large pores) of pores before and after immersion in external fluids. The relationship between the obtained pore distribution and relaxation time is shown in Fig. 8.

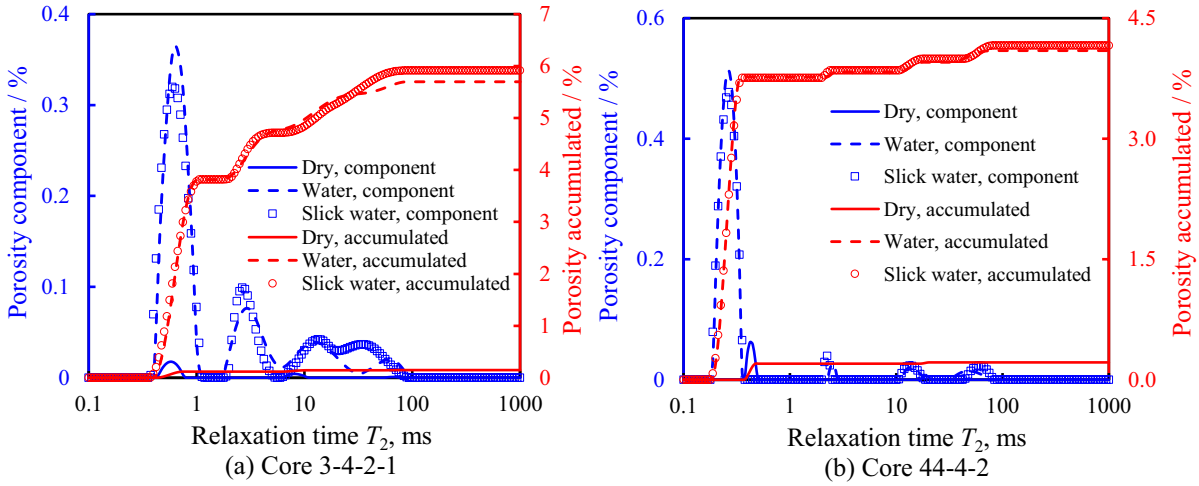

Fig. 8 Pore distribution characteristics of carbonaceous shale samples (core 3–4–2–1 and core 44–4–2) in their initial state and after soaking in backflow fluid

Table 8 The distribution of pore throats of different sizes in core 3–4–2–1 and core 44–4–2 before and after soaking in backflow fluid

Core No	Soaking fluid	Pore parameters	Distribution of pore throats of different sizes within the rock core				
			<0.01 μm	0.01–0.1 μm	0.1–1 μm	>1 μm	Total
3–4–2–1	Formation water	Porosity (pore volume/apparent core volume)%	3.79	0.99	0.69	0.23	5.70
		Porosity ratio (pore volume/total pore volume)%	66.61	17.31	12.06	4.02	100
	Backflow fluid	Porosity (pore volume/apparent core volume)%	3.79	0.92	0.86	0.34	5.91
		Porosity ratio (pore volume/total pore volume)%	64.14	15.57	14.51	5.77	100
44–4–2	Formation water	Porosity (pore volume/apparent core volume)%	3.77	0.17	0.12	0.15	4.10
		Porosity ratio (pore volume/total pore volume)%	91.98	1.63	2.82	3.57	100
	Backflow fluid	Porosity (pore volume/apparent core volume)%	3.75	0.10	0.14	0.17	4.16
		Porosity ratio (pore volume/total pore volume)%	90.22	2.35	3.40	4.03	100

As shown in Fig. 8, the total porosity of carbonaceous shale increases after saturation with backflow fluid. The total porosity of core 3–4 2–1 and core 44 4–2 saturattion with formation water are 5.70% and 4.10%, respectively. After saturation with backflow fluid, the total porosity are 5.91% and 4.16%, respectively, increasing by 0.21% and 0.06%. The increase in total porosity refers to an increase in the porosity of the fluid, which are 3.78% and 1.54%, respectively.

Table 8 presents the quantitative characterization results of pore distribution in cores 3–4 2–1 and 44 4–2 after immersion in backflow fluid. According to Table 8, it can be seen that after the interaction between carbonaceous shale and backflow fluid, the number of mesoscale and macroscale pores increases, while the number of microscale and nanoscale pores slightly decreases. The number of small pores changes, while the porosity of macroscale pore increases. After saturation with formation water, the macroscale pore porosity of core 3–4 2–1 and core 44 4–2 are 0.23% and 0.15%, respectively; after saturation with backflow fluid, the macroscale pore porosity are 0.34% and 0.17% respectively, and the variation values of macroscale pore porosity are 0.11% and 0.02%, with an increase of 14.45–49.16%. After saturation with backflow fluid, the microscale pore porosity of core 3–4 2–1 and core 44 4–2 decreased by 0–0.02%, the small pore porosity changed by −0.07–0.03%, the mesoscale pore porosity increased by 0.02–0.17%, the microscale pore decreased by 0.07–0.40%, the small pore changed by −6.61–46.59%, and the mesoscale pore increased by 22.43–24.86%.

Table 9 summarizes the evaluation results of the sensitivity of the pore structure of core 3–4–2–1 and core 44–4–2 to backflow fluid. According to Table 9, it can be seen that the backflow fluid is insensitive to the total porosity of carbonaceous shale, weakly harms microscale and nanoscale pores with moderate to weak improvement, and weakly improves small/medium/large pores with moderate to weak improvement. In summary, the results of this study indicate that the backflow fluid is not sensitive to the total porosity of carbonaceous shale, but has weak damage to microscale and nanoscale pores with moderate improvement, and weak to moderate improvement on small pores, mesoscale pore, and macroscale pore.

5 Conclusions

In this paper, firstly, taking pure shale as the research object, the influence mechanism of slick water and backflow fluid on the pore throat structure of pure shale is explored. Then, taking carbonaceous shale as the research object, the mechanism of the influence of slick water and backflow fluid on the pore throat structure of carbonaceous shale is analyzed. Finally, a comparative analysis and summary are conducted on the sensitivity of different types of shale to external fluids. Key findings are summarized below:

(a) Based on the sensitivity test results of foreign fluids on different types of shale, it was found that slick water has a harmful effect on the total porosity of different types of shale. The change rate is manifested as carbonaceous shale (−7.1%) > pure shale (−1.6%).
(b) For slick water, the decrease in macropores is the largest, followed by mesopores and micro/nano pores. The average reduction in macropores and micro/nano pores of carbonaceous shale is 90.0% and 5.0%, while the average reduction

Table 9 Evaluation results of the sensitivity of pore structures in core 3–4–2–1 and core 44–4–2 to backflow fluid

Core No	Soaking fluid	Evaluating indicator	I	Imic (< 0.01 μm)	Imc (0.01 ~ 0.1 μm)	Ime (0.1 ~ 1 μm)	Ima (> 1 μm)
3–4–2–1	Backflow fluid	Indicator value	3.78	−0.07	−6.61	24.86	49.16
		Impact level	None	None	Weak (damage)	Weak (improved)	Moderately weak (improved)
44–4–2	Backflow fluid	Indicator value	1.54	−0.40	46.59	22.43	14.45
		Impact level	None	None	Moderately weak (improved)	Weak (improved)	Weak (improved)

in macropores and mesopores of pure shale is 17.7% and 6.8%.

(c) After the action of backflow fluid, the total porosity of different types of shale is not sensitive. The rate of change satisfies: carbonaceous shale (+2.7%) > pure shale (+1.6%). The maximum increase is in large pore.

(d) For backflow fluid, the average increase in macroscale pore, mesoscale pore, and small pore of carbonaceous shale are 31.8%, 23.6%, 20.2%, respectively; the average increase in macroscale pore of pure shale is 17.1%.

Author contribution YY, JW, YL: Supervision, reviewing and editing; YY, JW, YL, QZ, JL, JL: Investigation, writing, project administration.

Funding Natural Science Foundation of Heilongjiang Province (Grant No. LH2022E019) and China Postdoctoral Science Foundation (Grant No. 2022M710594).

Availability of data and materials Data is available on request.

Declarations

Ethics approval and consent to participate The authors declare that the submitted work is original and has not been submitted to more than one journal for simultaneous consideration.

Consent to publish The authors agree to publication in the Geomechanics and Geophysics for Geo-Energy and Geo-Resources and also to publication of the article in English by Springer in Springer's corresponding English-language journal.

Competing interest There is no competing interests.

References

Assal EM, Farouk S, Sarhan MA (2023) Sedimentary facies controls on reservoir quality of the Abu Madi Formation, offshore Nile Delta Basin, Egypt. Geomech Geophys Geo-Energy Geo-Resour 9:130. https://doi.org/10.1007/s40948-023-00670-9

Chen M, Lu Y, Kang Y, Zhang T, Zhang X, Chen Z, You L, Li Y (2020) Parameters selection for experiment on aqueous phase trapping damage in shale gas reservoirs. J Natl Gas Sci Eng 83:103551. https://doi.org/10.1016/j.jngse.2020.103551

Chen J, Che Z, Su X, Zhou L, Liu X, Zhang L (2023) Nonlinear flow and permeability anisotropy characteristics in hydraulic fracturing-induced rock fractures subjected to various normal compressive stresses. Geomech Geophys Geo-Energy and Geo-Resour 9:49. https://doi.org/10.1007/s40948-023-00583-7

Cui J, Yang J, Wang M, Wang X, Wu Y, Yu C (2023) Shale porosity prediction based on random forest algorithm. Petrol Geol Recov Effic 30(6):13–21. https://doi.org/10.13673/j.pgre.202212025

Ding X, You Q, Wu J, Zhang J, Liu J, Dai C, Sun N, Wei L, Sun Y (2023) Hydration characteristics and mechanism study of artificial fracture surface in illite rich shale gas reservoir: a case study of Longmaxi formation shale in Yongchuan District. Energy Rep 9:4174–4186. https://doi.org/10.1016/j.egyr.2023.03.064

Elbahrawy A, Omran MA, Khamees H, Sarhan MA (2023) Geophysical structural interpretation of Esh El Mallaha basin, southern Gulf of Suez: implications for oil potential in South Malak and Rabeh fields. Geomech Geophys Geo-Energy Geo-Resour 9:58. https://doi.org/10.1007/s40948-023-00605-4

Gao XH, Liu JX, Shang XC et al (2023) A semi-analytical approach to nonlinear multi-scale seepage problem in fractured shale gas reservoirs with uncertain permeability distributions. Gas Sci Eng 110:104841. https://doi.org/10.1016/j.jngse.2022.104841

Guo J, Li Y, Wang S (2018) Adsorption damage and control measures of slick-water fracturing fluid in shale reservoirs. Pet Explor Dev 45(2):336–342. https://doi.org/10.1016/S1876-3804(18)30037-5

Guo X, Sun X, Mu J, Qiao H, Guo Q, He P, Luo P, Wang X (2023) Experimental study on the effect of CO_2–water on shale pore structure. Unconventional Oil Gas 10(06):116–122. https://doi.org/10.19901/j.fcgyq.2023.06.16

Hou B, Wang Y, Zhang Y, You Y (2023) Regional evaluation method of ground stress in shale oil reservoirs-taking the Triassic Yanchang formation in northern Shaanxi area as an example. Geomech Geophys Geo-Energy Geo-Resour 9:140. https://doi.org/10.1007/s40948-023-00665-6

Jiang XW, Chen M, Li QH et al (2022) Study on the feasibility of the heat treatment after shale gas reservoir hydration fracturing. Energy 254(Part B):124422. https://doi.org/10.1016/j.energy.2022.124422

Lai N, Fan W, Zhang X, Liu L, Zhou X, Chen S (2023) Temperature-sensitive polymer based nano-SiO_2 composite

multi-component synergistic improvement of shale stability in water-based drilling fluids. Geoenergy Science and Engineering 224:211498. https://doi.org/10.1016/j.geoen.2023.211498

Li GL, Li GF, Luo C et al (2023) Dynamic evolution of shale permeability under coupled temperature and effective stress conditions. Energy 266:126320. https://doi.org/10.1016/j.energy.2022.126320

Liu B, Wang H, Fu X, Bai Y, Bai L, Jia M, He B (2019) Lithofacies and depositional setting of a highly prospective lacustrine shale oil succession from the Upper Cretaceous Qingshankou Formation in the Gulong Sag, northern Songliao Basin, Northeast China. AAPG Bull 103:405–432. https://doi.org/10.1306/08031817416

Liu H, Kuang L, Li G, Wang F, Jin X, Tao J, Meng S (2020a) Considerations and suggestions on optimizing completion methods of continental shale oil in China. Acta Petrolei Sinica 41(04):489–496

Liu B, Yang Y, Li J, Chi Y, Li J, Fu X (2020b) Stress sensitivity of tight reservoirs and its effect on oil saturation: A case study of Lower Cretaceous tight clastic reservoirs in the Hailar Basin, Northeast China. J Petrol Sci Eng 184:106484. https://doi.org/10.1016/j.petrol.2019.106484

Liu B, Song Y, Zhu K, Su P, Ye X, Zhao W (2020c) Mineralogy and element geochemistry of salinized lacustrine organic-rich shale in the Middle Permian Santanghu Basin: Implications for paleoenvironment, provenance, tectonic setting and shale oil potential. Mar Pet Geol 120:104569. https://doi.org/10.1016/j.marpetgeo.2020.104569

Liu B, Sun J, Zhang Y, He J, Fu X, Yang L, Xing J, Zhao X (2021) Reservoir space and enrichment model of shale oil in the first member of Cretaceous Qingshankou Formation in the Changling sag, southern Songliao Basin. NE China Petrol Explorat Develop 48(3):608–624. https://doi.org/10.1016/S1876-3804(21)60049-6

Liu B, Mohammadi M, Ma Z, Bai L, Wang L, Xu Y, Ostadhassan M, Hemmati-Sarapardeh A (2023a) Evolution of porosity in kerogen type I during hydrous and anhydrous pyrolysis: experimental study, mechanistic understanding, and model development. Fuel 338:127149. https://doi.org/10.1016/j.fuel.2022.127149

Liu H, Huang Y, Cai M, Meng S, Tao J (2023b) Practice and development suggestions for hydraulic fracturing technology in the Gulong shale oil reservoirs in Songliao Basin. NE China Petrol Explorat Develop 50(03):603–612. https://doi.org/10.1016/S1876-3804(23)60420-3

Liu H, Meng SW, Wang SL et al (2023c) Mechanical characteristics and fracture propagation mechanism of the Gulong shale. Oil Gas Geol 44(04):820–828

Liu X, Meng S, Liang Z, Tang C, Tao J, Tang J (2023d) Microscale crack propagation in shale samples using focused ion beam scanning electron microscopy and three-dimensional numerical modeling. Pet Sci 20(3):1488–1512. https://doi.org/10.1016/j.petsci.2022.10.004

Lu Y, Wang Y, Zhang J et al (2020) Investigation on the characteristics of pyrolysates during co-pyrolysis of Zhundong coal and Changji oil shale and its kinetics. Energy 200:117529. https://doi.org/10.1016/j.energy.2020.117529

Ma L, Dowey PJ, Rutter E et al (2019) A novel upscaling procedure for characterizing heterogeneous shale porosity from nanometer-to millimetre-scale in 3D. Energy 181:1285–1297. https://doi.org/10.1016/j.energy.2019.06.011

Men Y, Zhang H, Yan J, Kang J, Xiong G, Ma L, Cao J (2023) Characteristics of specific surface area of organic-rich shale in Niutitang Formation in southeastern Guizhou. Unconventional Oil Gas 10(05):24–29. https://doi.org/10.19901/j.fcgyq.2023.05.04

Meng S, Li D, Liu X, Zhang Z, Tao J, Yang L, Rui Z (2023a) Study on dynamic fracture growth mechanism of continental shale under compression failure. Gas Science and Engineering 114:2949–9089. https://doi.org/10.1016/j.jgsce.2023.204983

Meng SW, Zhang ZH, Tao JP et al (2023b) A novel upscaling method for evaluating mechanical properties of the shale oil reservoir based on cluster analysis and nanoindentation. J Energy Res Technol 145(11):112901

Namaee-Ghasemi A, Ayatollahi S, Mahani H (2023) Insights into the effects of pore structure, time scale, and injection scenarios on pore-filling sequence and oil recovery by low-salinity waterflooding using a mechanistic DLVO-Based Pore-Scale Model. SPE J 28(04):1760–1776. https://doi.org/10.2118/214320-PA

Nie B (2023) Study on thermal decomposition of oil shale: two-phase fluid simulation in wellbore. Energy 272:127124. https://doi.org/10.1016/j.energy.2023.127124

Shao JX, You LJ, Jia N et al (2023) Salt crystal: Natural proppant for enhancing shale reservoir production. Energy 262(Part B):125569. https://doi.org/10.1016/j.energy.2022.125569

Shi WR, Zhang CM, Jiang S et al (2022) Study on pressure-boosting stimulation technology in shale gas horizontal wells in the Fuling shale gas field. Energy 254(Part B):124364. https://doi.org/10.1016/j.energy.2022.124364

Sun F, Yao Y, Chen M, Li X, Zhao L, Meng Y, Sun Z, Zhang T, Feng D (2017) Performance analysis of superheated steam injection for heavy oil recovery and modeling of wellbore heat efficiency. Energy 125:795–804. https://doi.org/10.1016/j.energy.2017.02.114

Sun F, Yao Y, Li X (2018a) The heat and mass transfer characteristics of superheated steam coupled with non-condensing gases in horizontal wells with multi-point injection technique. Energy 143:995–1005. https://doi.org/10.1016/j.energy.2017.11.028

Sun F, Yao Y, Li G, Li X (2018b) Geothermal energy extraction in CO_2 rich basin using abandoned horizontal wells. Energy 158:760–773. https://doi.org/10.1016/j.energy.2018.06.084

Tao J, Meng S, Li D, Rui Z, Liu H, Xu J (2023) Analysis of CO_2 effects on porosity and permeability of shale reservoirs under different water content conditions. Geoenergy Sci Eng 226:2949–8910. https://doi.org/10.1016/j.geoen.2023.211774

Wang B, Liu B, Yang J, Bai L, Li S (2022a) Compatibility characteristics of fracturing fluid and shale oil reservoir: A case study of the first member of Qingshankou Formation, northern Songliao Basin, Northeast China. J Petrol Sci

Eng 211:110161. https://doi.org/10.1016/j.petrol.2022.110161

Wang K, Jiang B, Ye K, Li H, Tan Y (2022b) Spontaneous imbibition model for micro-nano-scale pores in shale gas reservoirs considering gas–water interaction. J Petrol Sci Eng 209:109893. https://doi.org/10.1016/j.petrol.2021.109893

Wei ZJ, Sheng JJ (2022) Changes of pore structures and permeability of the Chang 7^3 medium-to-low maturity shale during in-situ heating treatment. Energy 248:123609. https://doi.org/10.1016/j.energy.2022.123609

Wei JG, Zhang A, Li JT et al (2023a) Study on microscale pore structure and bedding fracture characteristics of shale oil reservoir. Energy 278(Part A):127829. https://doi.org/10.1016/j.energy.2023.127829

Wei J, Fu L, Zhao G, Zhao X, Liu X, Wang A, Wang Y, Cao S, Jin Y, Yang F, Liu T, Yang Y (2023b) Nuclear magnetic resonance study on imbibition and stress sensitivity of lamellar shale oil reservoir. Energy 282:128872. https://doi.org/10.1016/j.energy.2023.128872

Xiao W, Yang Y, Huang C, Xie Q, Chen X, Cao R, Zheng L, Ren J (2023) Rock wettability and its influence on crude oil producing characteristics based on NMR technology. Petrol Geol Recov Effic 30(1):112–121. https://doi.org/10.13673/j.cnki.cn37-1359/te.202109016

Xie WD, Wang M, Chen S et al (2022) Effects of gas components, reservoir property and pore structure of shale gas reservoir on the competitive adsorption behavior of CO_2 and CH_4. Energy 254(Part B):124242. https://doi.org/10.1016/j.energy.2022.124242

Xie Y, Liu H, Zhang K, Jia W, Li J, Meng X (2023) Dynamic evaluation of microscopic damage and fluid flow behavior in reservoir shale under deviatoric stress. Energy 283:128391. https://doi.org/10.1016/j.energy.2023.128391

Yang K, Zhou JP, Xian XF et al (2022a) Chemical-mechanical coupling effects on the permeability of shale subjected to supercritical CO_2-water exposure. Energy 248:123591. https://doi.org/10.1016/j.energy.2022.123591

Yang XY, Cai JH, Jiang GS et al (2022b) Modeling of nanoparticle fluid microscopic plugging effect on horizontal and vertical wellbore of shale gas. Energy 239(Part B):122130. https://doi.org/10.1016/j.energy.2021.122130

Yang S, Li X, Zhang K, Yu Q, Du X (2022c) The coupling effects of pore structure and rock mineralogy on the pre-Darcy behaviors in tight sandstone and shale. J Petrol Sci Eng 218:110945. https://doi.org/10.1016/j.petrol.2022.110945

Yang X, Xie J, Ye X et al (2023a) Sealing characteristics and discrete element fluid dynamics analysis of nanofiber in nanoscale shale pores: Modeling and prediction. Energy 273:127229. https://doi.org/10.1016/j.energy.2023.127229

Yang H, Wang L, Yang C, Guo W, Bi Z, Guo Y (2023b) Experimental investigation on different effects of fracturing fluids on mechanical properties and failure mechanism of continental shale. Int J Rock Mech Min Sci 164:105362. https://doi.org/10.1016/j.ijrmms.2023.105362

Yu H, Xu W, Li B, Huang H, Micheal M, Wang Q, Huang M, Meng S, Liu H, Wu H (2023) Hydraulic fracturing and enhanced recovery in shale reservoirs: theoretical analysis to engineering applications. Energy Fuels 37(14):9956–9997. https://doi.org/10.1021/acs.energyfuels.3c01029

Yuan B, Zhao ZM, Meng SW et al (2023) Intelligent identification and real-time warning method of diverse complex events in horizontal well fracturing. Pet Explor Dev 50(5):1–9

Zhou Y, You L, Kang Y, Xie B, Cheng Q (2022) Experimental study of the fracture initiation through the synergy of spontaneous imbibition and hydration of residual fracturing fluids in shale gas reservoirs. J Natl Gas Sci Eng 102:104577. https://doi.org/10.1016/j.jngse.2022.104577

Zhou X, Wei J, Zhao J, Zhang X, Fu X, Shamil S, Abdumalik G, Chen Y, Wang J (2024) Study on pore structure and permeability sensitivity of tight oil reservoirs. Energy 288:129632. https://doi.org/10.1016/j.energy.2023.129632